

BNL 7-foot bubble chamber experiment - Neutrino deuterium interactions

K. Furuno^{a*}

in collaboration with

A. Suzuki^a, T. Kitagaki^b, M. Etou^a, H. Sagawa^c, K. McConnel^{c†}, E. J. Jeon^{c‡}, and M. Sakuda^c

^aRCNS, Research Center for Neutrino Science, Graduate School of Science, Tohoku University,
Aoba-ku, Aramaki, Sendai 980-8578, Japan

^bTGU, Tohoku Gakuin University,
Chuou 1-13-1, Tagajou 985-8537, Miyagi, Japan

^cKEK, Institute of Particle and Nuclear Studies.,
Oho 1-1, Tsukuba 305-0801, Japan

BNL neutrino experiment data is currently the most precise in the world and still outstanding in the low energy region of 1-2 GeV. Its high quality has made precise comparisons possible with theoretical models of interactions [3,4,6–10]. The quasi-elastic and single pion (Δ^{++}) channels have been extensively studied in the past in comparison with theoretical models [11–14]. In this paper the experimental details of the past analyses for the single pion channel are summarized. Then the comparisons of the data with the Rein-Sehgal model [16] are presented.

1. Introduction

Among the efforts made at NuInt Workshops for the future precise accelerator neutrino oscillation experiments, comparisons between the existing neutrino data in the world and the theoretical models were presented during the NuInt01/02 sessions and the importance of comparisons of the exclusive channels of the past experimental data in the sub-GeV region to the newly tuned theoretical models were addressed [1,2].

The BNL 7-foot bubble chamber neutrino experiment currently provides the highest precision data on the exclusive channels in the low energy range of 1-2 GeV [3,4,6–10]. Detailed comparisons of the outstanding BNL data to the updated theoretical calculations should be performed. In this paper I will outline the BNL experiment and summarize the results of analyses, and then discuss the comparison of the $\nu D \rightarrow \mu^- p \pi^+ n_s$ data with the theoretical model from Rein-Sehgal [16]. Previously, we compared our data

[3,6,7] with the theoretical Adler model [12] calculation from Scheiner-von Hippel [13]. These two models are most commonly used by the neutrino experiments.

2. The experiment

The experiment has been performed at Brookhaven National Laboratory (BNL) using the 7-foot bubble chamber filled with deuterium exposed to the Alternating Gradient Synchrotron (AGS) wide-band neutrino beam with an average energy of 1.6 GeV. The muon neutrino beam direction at the bubble chamber was known to be within about 0.5 degree. Other flavors and anti-neutrinos were negligible. Details of experimental arrangement are found in the papers [3,4]. Brief summary is given in the following sentences.

Two periods of runs in 1976-1977 (0.99 M pictures) and 1979-1980 (0.8 M pictures) were held and the total of 1.8 M pictures were obtained. The studies of this article were based on the final total event sample.

In this experiment the neutrino flux was not independently measured and thus the results provided the

*furuno@awa.tohoku.ac.jp

†Present address; Columbia University, 2960 Broadway, New York, NY 10027-6902, USA

‡Present address; Seoul National University, Seoul 151-742, Korea

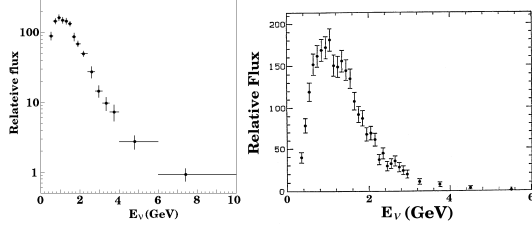


Figure 1. Left : Relative neutrino flux obtained from quasi-elastic events at $M_A^{QE} = 1.07\text{GeV}/c^2$ [3]. Right : Same as left but doubled statistics at $M_A^{QE} = 1.1\text{GeV}/c^2$ [5].

flux independent analyses and model dependent cross sections.

Fig. 1 shows the shape of the neutrino flux, which peaks at 1.1-1.2 GeV and covers the Δ resonance regions, obtained by the best fit axial vector mass of $M_A^{QE} = 1.07\text{GeV}/c^2$ from the first run [3] and $M_A^{QE} = 1.1\text{GeV}/c^2$ from both runs [5] respectively on the quasi-elastic events.

The bubble chamber dimension showed approximately 12' height and 7' diameter cylinder coated by the light reflector on the inner wall, equipped with three 70 mm cameras and operated in a 25 kG magnetic field, which allowed the geometrical four momentum reconstructions in high resolutions of the event tracks measured on the three viewed films. The typical momentum resolution was about 2-3% for the track length longer than 40 cm.

Four stainless steel plates were mounted in the downstream region of the chamber as shown in Fig. 2 in order for the particle identifications. Hence the visible volume in the chamber was about 5 – 6m³. Fig. 3 shows the picture of inside chamber taken by the camera view 2.

All the tracks were examined for the particle identification by means of the observations of the energy loss in the liquid (*e.g.*, bubble densities, track curvatures, knock on electrons, *etc.*) and the interactions with the hard materials.

Fig. 4 shows the proton-pion separation (a) in all the measured positively charged tracks and the μ^- identification (b) in the kinematically reconstructed

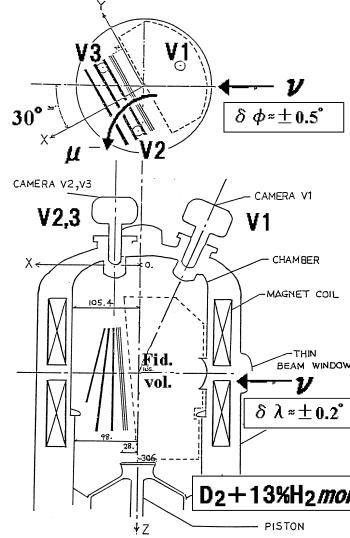


Figure 2. Schematic cross section of the BNL 7-foot bubble chamber.

(three constraint fits) charged current events [5]. As the results, precision analyses of the exclusive channels have become available.

3. Data samples of quasi-elastic (QE) and single pion (1π) channels

The procedures of the film scanning, measuring and the charged current event selections were described in detail in the previously published papers [3, 5–7]. Also the backgrounds which come from inter-channel confusions, hydrogen contaminations, neutral current and hadron interactions were discussed in detail and some additional informations may be found in ref.'s [4,8,9] and [10].

3.1. Selection of the charged current events

All the film was scanned to find events with at least one charged track whose vertex started in the liquid. About 32% of the film was scanned twice. Topology dependent scanning efficiency as the functions of number of prongs (observed charged tracks) and Q^2 was obtained. The averaged scanning efficiency was 93% in which the single scanning efficiency was

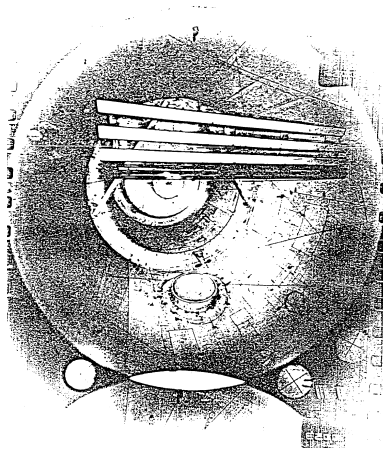


Figure 3. Chamber insight as seen on the camera view 2.

about 90%. All the 15 K events were measured, geometrically reconstructed and kinematical fittings were applied. The averaged measuring efficiency was 94%. Charged hadron induced backgrounds consistent with the pp and πp interactions or inconsistent with net charge of 0/+1 were rejected.

The charged current (CC) events were selected by requiring that the total visible momentum should be greater than 150 MeV/c, its direction to the incident neutrino should be within 50 degrees and at least one negatively charged track should not be inconsistent with muon hypothesis. Finally about 9 K CC events were obtained in the 4m^3 fiducial volume.

3.2. QE and 1 π

The exclusive channels were selected by 0-3 constraint kinematical fits and consistency with observed particle identifications. About 80% of positively charged tracks were identified uniquely as proton or pion and about 40% of muon tracks were identified as shown in Fig 4.

The QE and $p\pi^+n_s$ channels were required the consistency to the particle identifications and solved through three constraint (3C) fittings by means of chi-squared minimization to the kinematical topologies of the reactions, $\nu_\mu D \rightarrow \mu^- pp_s$ and $\nu_\mu D \rightarrow \mu^- p\pi^+n_s$, respectively, where the only major unknown param-

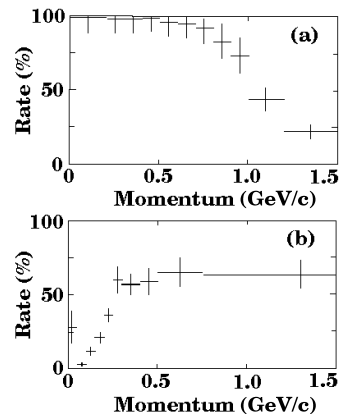


Figure 4. (a) $p - \pi$ separation. (b) μ^- identification.

ter was the incident neutrino energy. These events had two to three charged tracks (2,3-pronged) observed in the chamber according to the missing spectator proton p_s whose momentum was typically less than about 150 MeV/c.

In Fig 5 the distribution of the fit spectator proton momentum in the QE events was shown with the calculation of the Hulthen wave function which is entry normalized. The momentum of the missing spectator proton in two-pronged event was well within the order of the experimental resolution in its magnitude that provided strong constraint on the missing parameters and thus ensured the quality of the result of fitting.

The distribution of EMPX which is defined as, $[visible(energy - longitudinal momentum) - target nucleon mass] = - [missing(energy - longitudinal momentum) - spectator nucleon mass + binding energy]$,

is shown in Fig 5 for all the two-pronged events. Shaded area indicates the fit QE events, where EMPX approximately equals to the missing longitudinal momentum. It clearly shows the spread centered at zero due to the target fermi motion and the measured momentum resolution that indicates negligible systematic experimental bias and background within sensitivity.

Thus the missing momentum of the spectator neutron in the $p\pi^+n_s$ channel was well reconstructed be-

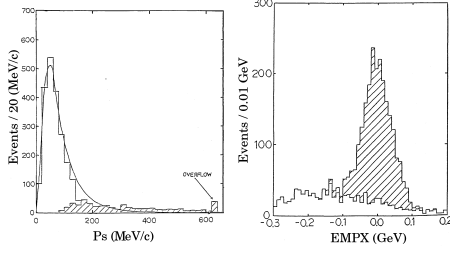


Figure 5. Left : Spectator proton momentum of the 3C-fit QE events. Unshaded area indicates the invisible protons. Right : EMPX of all two-pronged events. Shaded area indicates the fit QE events.

low 150 MeV/c [7].

The events with chi-square probability of greater than 1% were selected.

Other 1π channels, $\nu_\mu D \rightarrow \mu^- n \pi^+ p_s$ and $\nu_\mu D \rightarrow \mu^- p \pi^0 p_s$ were selected through the 0C fits with particle identifications. Only two-pronged events were used to avoid the ambiguity between recoil and spectator momentum. Because of kinematical nature of phase space with missing neutron and π^0 , 15% of those events have fit to both channels and were assigned to both with equal weights.

The final data samples of channels obtained were 2684 (QE), 1610 ($p\pi^+n_s$), 853.5 ($p\pi^0p_s$) and 822.5 ($n\pi^+p_s$) events, and the corrections to these numbers estimated were 1.06 ± 0.11 (1.11 ± 0.04 [7]), 1.12 ± 0.07 , 1.05 ± 0.14 and 0.89 ± 0.10 , respectively [6].

The corrections have come from the event losses in the scanning and measuring procedure, in the varieties of cuts, from the hydrogen contamination, from the ambiguities of fits between channels, from the contaminations from other multiple neutral production channels and the neutral current interactions, and from the hadron induced backgrounds.

The prong- and Q^2 -dependent corrections of the scanning efficiency to the QE events were applied for the calculations described in the following sections. Fig. 6 shows, for example, the averaged Q^2 dependent scanning efficiencies for the single and double scannings.

Details of examinations of these correction factors

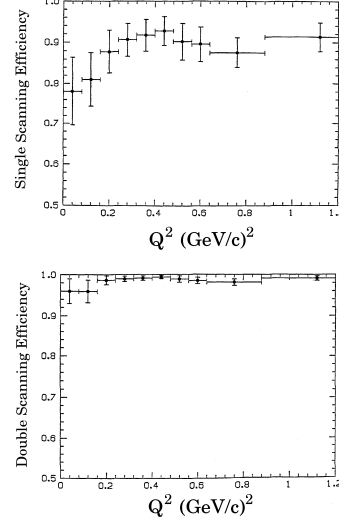


Figure 6. Averaged single (upper) and double (lower) scanning efficiencies as the functions of Q^2 .

were described in the ref.'s previously mentioned.

4. QE and 1π cross sections

4.1. QE cross section

The neutrino flux was analyzed with the QE sample by means of standard electro-weak form factor analysis [6,7] using the formalism of the nucleon cross section from C. H. L. Smith [11,12] with the correction of the deuteron effects [14] which takes into account the the Fermi motion and the Pauli exclusion principle through the hulthen wave function and the final state interaction.

With the assumptions of the vector mass $M_V = 0.84 \text{ GeV}/c^2$, the maximum likelyhood fit of the one parameter M_A^{QE} to the Q^2 distribution is performed with the event probability density function,

$$\left[N \times \phi(E_\nu) R^{\text{QE}}(Q^2) \frac{d\sigma_N^{\text{QE}}(M_A^{\text{QE}})}{dQ^2} \right]^{w^{\text{QE}}(Q^2, \text{prongs})}, \quad (1)$$

where the $\phi(E_\nu)$ is the neutrino Flux, $\sigma_N^{\text{QE}} = \sigma(\nu_\mu n \rightarrow \mu^- p)$ is the nucleon cross section, $R^{\text{QE}}(Q^2)$ is the correction factor for the deuteron effect and $w^{\text{QE}}(Q^2, \text{prongs})$ is the event weight as the inverse

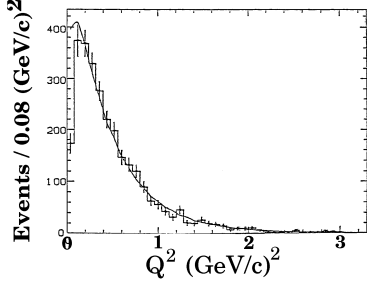


Figure 7. Q^2 distribution of the QE events (black circle) and the fit curve at $M_A^{\text{QE}} = 1.10 \text{ GeV}/c^2$ [5,6].

of the scanning efficiency which is prong- and Q^2 -dependent. The flux factor $\phi(E_\nu)$ is also included in the denominator of the normalization factor, N , and thus simply canceled out that allows the flux independent analysis of the M_A^{QE} .

Fig.4 of the ref.[14] shows the $R^{\text{QE}}(Q^2)$. It doesn't include the meson exchange current and the off-mass-shell effect. The nuclear effects are believed to become apparent for Q^2 below about $0.1 \text{ (GeV}/c)^2$. The E_ν dependencies were studied [5] and found some differences at low E_ν but were statistically insignificant. The effect of nucleon correlation was also studied using data sets with restricted spectator momentum and found no significant differences on the fit M_A^{QE} 's [7].

The M_A^{QE} was obtained as $1.10 \pm 0.05 \text{ GeV}/c^2$ for $0.08 < Q^2 < 3.0 \text{ (GeV}/c)^2$ [5,6] and $1.07 \pm 0.05 \text{ GeV}/c^2$ for $0.1 < Q^2 < 3.0 \text{ (GeV}/c)^2$ [7]. Fig. 7 shows the Q^2 distribution of the data with the fit curve at $M_A^{\text{QE}} = 1.10 \text{ GeV}/c^2$ [5,6]. The curve was calculated by integrating over the range of $0.3 < E_\nu < 6.0 \text{ GeV}$ [5] with flux obtained [3]. The data is weighted due to the prong- and Q^2 -dependent scanning efficiencies.

The effect of missing recoil proton at very low Q^2 was discussed in the ref.[7].

The updated analysis of M_A^{QE} using newly compiled electromagnetic form factors has been held and the result will be shown elsewhere [15].

4.2. 1π cross sections

The effective neutrino flux and the cross sections relative to QE from the data sample can be derived as

shown below.

$$d\sigma_{\text{D}}^{\text{QE}}(M_A^{\text{QE}}) = R^{\text{QE}}(Q^2)d\sigma_{\text{N}}^{\text{QE}}(M_A^{\text{QE}}), \quad (2)$$

$$\phi(E_\nu)\sigma_{\text{D}}^{\text{QE}}(M_A^{\text{QE}}) = \int \omega^{\text{QE}}(Q^2) \frac{d^2 N^{\text{QE}}}{dE_\nu dQ^2} dQ^2, \quad (3)$$

$$\frac{d\sigma_{\text{D}}^{1\pi}}{dQ^2} = \omega^{1\pi}(Q^2) \frac{d^2 N^{1\pi}}{dE_\nu dQ^2} \frac{1}{\phi(E_\nu)}, \quad (4)$$

where $\omega^{\text{QE}}(Q^2)$ and $\omega^{1\pi}(Q^2)$ are the event weights due to the number corrections and the prong- and Q^2 -dependent efficiencies which were described in the subsection 3.2.

Resulting single pion cross sections as a function of the neutrino energy were presented together with the multi-pion exclusive cross sections in the ref.[6] as shown in the talk. There all the errors due to statistics and M_A^{QE} were combined in quadratic manner.

In the ref.[6,7] theoretical Adler model [12] of $p\pi^+n_s$ channel developed by P. A. Schreiner and F. Von Hippel [13] was applied to the data sample in the way that the event probability density was calculated using the differential cross section as a function of both Q^2 and W^2 in the flux independent manner as described in the M_A^{QE} analysis. Resulting M_A^{Sch} was $1.28 \pm 0.1 \text{ GeV}/c^2$ for the ranges, $0.1 < Q^2 < 3 \text{ (GeV}/c)^2$, $1.08 < W = M(p\pi^+) < 1.4 \text{ GeV}/c^2$ and $0.5 < E_\nu < 6 \text{ GeV}/c^2$.

Detailed discussions of the experimental biases and the nuclear effects especially concerning to the spectator are found in the ref.[7]. Difference in the fit numbers of M_A^{Sch} was shown for the event set with restricted spectator momentum but was statistically insignificant.

4.3. Comparison with Rein-Sehgal predictions

From the equations (3) and (4) the ratio between QE and 1π cross sections leads to the flux independent comparison with theoretical predictions. The ratio $\sigma_{\text{D}}(p\pi^+n_s) / \sigma_{\text{D}}^{\text{QE}}(pp_s)$ (Schreiner[13] / (Smith[11] and Singh[14])) was compared using the fit values of M_A^{QE} and M_A^{Sch} to the data ratio, $N(p\pi^+n_s) / N(\text{QE})$ with the experimental corrections applied, as a function of E_ν [7], that showed good agreement within statistics. The comparison of the ratios as a function of Q^2 was also presented.

In this paper the Rein-Sehgal resonance model [16] was studied. Fig. 8 shows the Q^2 distribution of

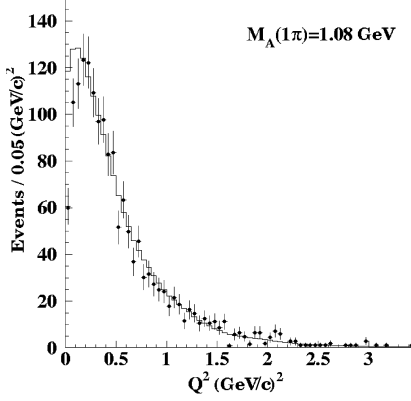


Figure 8. Q^2 distribution of $p\pi^+n_s$ events (black circle) with the best fit Rein-Sehgal model at $M_A^{\text{RS}} = 1.08 \text{ GeV}/c^2$ (solid histogram).

$p\pi^+n_s$ data with no W and E_ν cuts applied. The best fit M_A^{RS} to the Q^2 shape (integrated over the $W < 2.0 \text{ GeV}/c^2$) for $0.2 < Q^2 < 3 \text{ (GeV}/c^2)^2$ in the flux independent manner was obtained as $M_A^{\text{RS}} = 1.08 \pm 0.07 \text{ GeV}/c^2$ (statistical error only) without correction for the deuteron effects which is small (2-3%). The resulting calculated shape is shown on the plot as the solid histogram with the flux obtained from QE data at $M_A^{\text{QE}} = 1.07 \pm 0.05 \text{ GeV}/c^2$ and is entry normalized within the range of $0.2 < Q^2 < 3 \text{ (GeV}/c^2)^2$.

The Q^2 dependent correction to the data due to the scanning efficiency which is small ($< 5\%$) wasn't included and the systematic error due to this is within 2-3%. Good agreement was obtained for $Q^2 > 0.2 \text{ (GeV}/c^2)^2$ within experimental uncertainty.

The difference of the model calculation which is seen in the range of $Q^2 < 0.2 \text{ GeV}/c^2$ between the plots shown in the talk and the Fig. 8 is due to the differences of the lower limits of Q^2 used in the fits, where $0.1 \text{ GeV}/c^2$ was used on the plot in the talk.

Also the comparison is made in the cross section ratio as shown in Fig. 9 and best fit was obtained at $M_A^{\text{RS}} = 1.15_{-0.06}^{+0.08} \text{ GeV}/c^2$ (both statistical and QE error are included) with fixed $M_A^{\text{QE}} = 1.07 \pm 0.05 \text{ GeV}/c^2$. The experimental corrections were applied in the both of QE and 1π data. The data for 1π cross section again includes no W cut and the model was

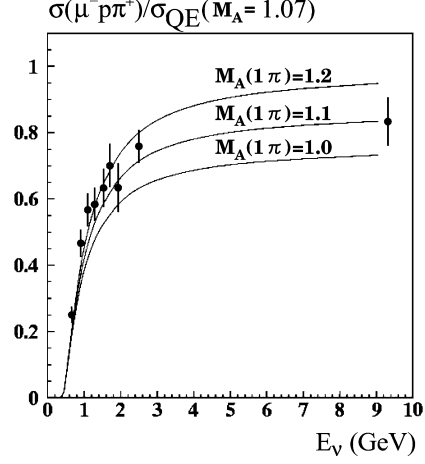


Figure 9. Cross section ratio between 1π and QE with the best fit Rein-Sehgal model at $M_A^{\text{RS}} = 1.15 \text{ GeV}/c^2$. The data (black circle) presents the ratio of deuteron cross sections. Solid curves represent the model with different M_A^{RS} 's.

calculated with $W < 2.0 \text{ GeV}/c^2$. The systematic effect due to this is within -10% . Deuteron effect was applied in the QE calculation, on the other hand it wasn't in the 1π model calculation and the systematic error due to this is about 2-3%.

In above two methods of analysis the non-updated vector form factors in the M_A^{QE} calculation were used. The difference from the calculation using the updated vector form factors will be discussed in future.

Despite of these systematic uncertainties in the theoretical calculations and in the experimental corrections to the data due to event losses in the low Q^2 region, good agreement in the above two different, flux independent method of M_A^{RS} estimations was obtained.

In the talk the cross section ratio for the channels $p\pi^0 p_s$ and $n\pi^+ p_s$ were presented together with Rein-Sehgal calculations. There included some systematic errors in the model calculations. Comparisons with newly tuned calculations are underway.

Because these two channels have large ambiguities in their visible kinematical topologies, about a

half of selected event sample comes from the background contaminations which are mainly the other CC channels, neutral current interactions and hadron incident interactions[6,7]. However the hadrons were estimated to be relatively small as about 15% for $p\pi^0 p_s$ and about 3% for $n\pi^+ p_s$. It requires the special cares in the precise comparisons with the model.

The cross section ratios from ANL data [17] were also calculated and shown in the talk with comments on that special cares should be taken for the fluxes used in the calculations of the cross sections when the cross sections but not directly the number of events themselves were used to compare. Otherwise it may possibly produce large systematic uncertainties.

5. Conclusion

The present BNL data was summarized especially according to the potential experimental biases in order for the detailed comparisons with theoretical models.

It was shown that the single pion data is still valuable and outstanding in respect to its statistics and quality in this low energy region. Especially the QE and the single pion data samples were compared with the Rein-Sehgal resonance model and obtained good agreement in the the axial vector masses calculated from the two different methods, the Q^2 shape and the cross section ratio analyses.

Further detailed comparisons between the model and the data for QE and multi-pion interactions with tuned nuclear effects, updated vector form factors and quark parton model will be performed.

ACKNOWLEDGEMENTS

I would like to thank the former BNL collaboration [18]. Their research was supported by the U.S.-Japan Cooperative Research Project on High Energy Physics under the Ministry of Education, Science, and Culture of Japan and the U.S. Department of Energy under Contract No. DE-AC02-76-CH00016. All rights of the data are reserved by the BNL collaboration.

REFERENCES

1. M. Sakuda, Nucl. Phys. **B Proc. Suppl.** **112**, 109(2002).
2. M. Sakuda, *to be published* in Nucl. Phys. **B Proc. Suppl.**, 2003.
3. N. J. Baker, *et al.*, Phys. Rev. **D23**, 2499(1981).
4. N. J. Baker, *et al.*, Phys. Rev. **D23**, 2495(1981).
5. H. Sagawa, Ph.D. thesis (1985), Tohoku Univ., Japan, *unpublished*.
6. T. Kitagaki, *et al.*, Phys. Rev. **D34**, 2554(1986).
7. T. Kitagaki, *et al.*, Phys. Rev. **D42**, 1331(1990).
8. N. J. Baker, *et al.*, Phys. Rev. **D25**, 617(1982).
9. G. L. Fogli, *et al.*, Phys. Rev. **D25**, 1436(1982).
10. N. J. Baker, *et al.*, Phys. Rev. **D28**, 2900(1983).
11. C. H. Llewellyn Smith, Phys. Rep. **C3**, 261(1971).
12. S. L. Adler, Ann. Phys. (N.Y.) **50**, 189(1968) and Phys. Rev. **D12**, 2644(1975).
13. P. A. Schreiner and F. Von Hippel, Nucl. Phys. **B58**, 333 (1973) and Phys. Rev. Lett. **30**, 339(1973).
14. S. K. Singh, Nucl. Phys. **B36**, 419(1971).
15. M. Sakuda, Proceedings of the 4th International Workshop on Neutrino Oscillations and their Origin, NOON2003 (Feb. 2003), Kanazawa, Japan, *to be published by World Scientific in Fall 2003*.
16. D. Rein and L. M. Sehgal, Ann. Phys. (N.Y.) **133**, 79(1981) and Z. Phys. **C35**, 43(1987).
17. S. J. Barish, *et al.*, Phys. Rev. **D16**, 3103(1977), K. L. Miller, *et al.*, Phys. Rev. **D25**, 1161(1982) and Y. Cho, *et al.*, Phys. Rev. **D4**, 1967(1971).
18. *The former BNL 7' BC Neutrino Experiment Collaboration* :
T. Kitagaki⁴, H. Yuta¹, S. Tanaka¹, A. Yamaguchi, K. Abe¹, K. Hasegawa⁵, K. Tamai⁶, H. Sagawa³, K. Furuno and K. Tamae ; *Bubble Chamber Physics Laboratory, Tohoku University, Sendai 980, Japan*,⁷
M. Higuchi and M. Sato ; *Tohoku Gakuin University, Chuou 1-13-1, Tagajou 985-8537, Japan*,
S. A. Kahn, M. Murtagh, R. B. Palmer, N. P. Samios, and M. Tanaka ; *Brookhaven National Laboratory, Upton, New York 11973, USA*.

⁴Currently TGU, Tohoku Gakuin University, Chuou 1-13-1, Tagajou 985-8537, Miyagi, Japan.

⁵Currently Nagoya University, Nagoya, Japan.

⁶Currently KEK, Institute of Particle and Nuclear Studies., Oho 1-1, Tsukuba 305-0801, Japan.

⁷Currently RCNS, Research Center for Neutrino Science, Graduate School of Science, Tohoku University, Aoba-ku, Aramaki, Sendai 980-8578, Japan.